Supplementary Material
Orbital Picture of Yu-Shiba-Rusinov Multiplets

Michael Ruby,[1] Yang Peng,[2] Felix von Oppen,[2] Benjamin W. Heinrich,[1] and Katharina J. Franke[1]
[1] *Fachbereich Physik, Freie Universität Berlin, 14195 Berlin, Germany*
[2] *Dahlem Center for Complex Quantum Systems and Fachbereich Physik, Freie Universität Berlin, 14195 Berlin, Germany*

THEORETICAL BACKGROUND

The Manganese (Mn) adatoms are presumably in a $^6S_{5/2}$ configuration. When placed in an isotropic environment, this implies that the exchange interaction is with the $l = 2$ conduction electrons and conserves angular momentum [1]. Lifting the degeneracy between the d-levels is the result of crystal-field splittings reflecting the anisotropy of the host, and the resulting multiplicities are largely determined by symmetry considerations. The splittings as well as the orbital dependence of the hybridization imply that the exchange and potential couplings between magnetic impurity and conduction electrons become orbital dependent.

When the magnetic impurity is placed in an isotropic superconductor, one thus expects five pairs of degenerate YSR states. Similar to the d-levels, the YSR states will split due to the symmetry reduction by crystal fields. One way of thinking about this splitting is as a result of the modification of the d-level energies and hybridizations mentioned above. Alternatively, we can first compute the Shiba states for a completely isotropic environment and then consider their splitting resulting from the symmetry reduction. As the results are controlled by group theory, both approaches give identical results as long as we do not attempt to compute specific values of energy levels. In the following, we briefly sketch the second approach.

Yu-Shiba-Rusinov states

Let us consider a homogeneous s-wave superconductor whose Hamiltonian in real space can be written as

$$H_s = \int dr \left\{ \sum_\sigma \psi_\sigma^\dagger(\mathbf{r}) \left[\frac{-\nabla^2}{2m} - \mu \right] \psi_\sigma(\mathbf{r}) + \Delta^* \psi_\uparrow(\mathbf{r}) \psi_\downarrow(\mathbf{r}) + \Delta \psi_\downarrow^\dagger(\mathbf{r}) \psi_\uparrow^\dagger(\mathbf{r}). \right\} \tag{S1}$$

Here $\psi_\sigma(\mathbf{r})$ annihilates an electron with spin σ at position $\mathbf{r}$, Δ is the superconducting order parameter and μ is the chemical potential. It is convenient to represent the electron field operators in the basis of spherical waves centered at the position of the impurity atom, namely

$$\psi_\sigma(\mathbf{r}) = \sum_{klm} c_{klm\sigma} \phi_{klm}(\mathbf{r}), \tag{S2}$$

where

$$\phi_{klm}(\mathbf{r}) = j_l(kr) Y_l^m(\hat{\mathbf{r}}), \quad m = -l, -l+1, \dots l \tag{S3}$$

with $l \in \mathbb{N}_0$, j_l the spherical Bessel function of order l, and Y_l^m the spherical harmonics of degree l and order m. Thus, we decompose the electrons in the superconductor into different angular-momentum channels,

$$H_s = \sum_{klm} c_{klm\sigma}^\dagger c_{klm\sigma} \xi_k + (-)^m \left[\Delta c_{klm\uparrow} c_{kl-m\downarrow} + \Delta c_{kl-m\downarrow}^\dagger c_{klm\uparrow}^\dagger \right] \tag{S4}$$

$$\xi_k = \frac{k^2}{2m} - \mu. \tag{S5}$$

In the situation we are considering here, the impurity atom is Mn^{++}, whose ground state is $^6S_{5/2}$ with a half-filled $3d$ shell. It was shown [1, 2] that, to lowest order, only the $l = 2$ channel electrons get scattered due to the impurity. Hence, in the following, we will only include the $l = 2$ conduction electrons in the Hamiltonian, and suppress this index. The full Hamiltonian including the impurity becomes

$$H = \sum_{m=-2}^{2} \left\{ \sum_{k\sigma} c_{km\sigma}^\dagger c_{km\sigma} \xi_k + (-)^m \sum_k \left(\Delta c_{km\uparrow} c_{k-m\downarrow} + \Delta c_{k-m\downarrow}^\dagger c_{km\uparrow}^\dagger \right) \right\} + \sum_{\sigma\sigma'} \sum_{kk'} \left(J\mathbf{S} \cdot \boldsymbol{\sigma}_{\sigma\sigma'} + V\delta_{\sigma\sigma'} \right) c_{km\sigma}^\dagger c_{km\sigma'}, \tag{S6}$$

where J and V are the strengths of the exchange the potential coupling between the impurity atom and the conduction electrons. If we assume the impurity spin $\mathbf{S}$ to be aligned along z direction, the last term in the Hamiltonian can be written as

$$JS(c^\dagger_{km\uparrow}c_{km\uparrow} - c^\dagger_{km\downarrow}c_{km\downarrow}).$$

Introducing Nambu spinor $C_{km} = (c_{km\uparrow}, c^\dagger_{k-m\downarrow})^T$, we have the Bogoliubov–de Gennes Hamiltonian

$$H = \sum_{m=-2}^{2} \left\{ \sum_k C^\dagger_{km} \mathcal{H}_s C_{km} + \sum_{kk'} (JS + V\tau_z)\, C^\dagger_{km} C_{k'm} \right\} \tag{S7}$$

$$\mathcal{H}_s = \xi_k \tau_z + (-)^m \Delta \tau_x. \tag{S8}$$

Here, τ_α denotes Pauli matrices in particle-hole space.

The Green function corresponding to the above Hamiltonian fulfills the Dyson equation

$$G_{kk'm}(E) = g_{km}(E)\delta_{kk'} + g_{km}(E)\,(JS + V\tau_z) \sum_{k_1} G_{k_1 k'm}(E), \tag{S9}$$

where g_{km} is the Green function of the homogeneous superconductor without the impurity,

$$g_{km}(E) = (E - \xi_k\tau_z - (-)^m\Delta\tau_x)^{-1} = \frac{E + \xi_k\tau_z + (-)^m\Delta\tau_x}{E^2 - \xi_k^2 - \Delta^2}. \tag{S10}$$

In particular, we have

$$\sum_k G_{kk'm}(E) = g_{k'm}(E) + \left[\sum_k g_{km}(E)\right] (JS + V\tau_z) \left[\sum_{k_1} G_{k_1 k'm}(E)\right], \tag{S11}$$

which gives

$$G_{kk'm}(E) = g_{km}(E)\delta_{kk'} + (JS + V\tau_z) g_{km}(E) \left[1 - \sum_k g_{km}(E)(JS + V\tau_z)\right]^{-1} g_{k'm}(E). \tag{S12}$$

One can identify the T matrix as

$$T(E) = (JS + V\tau_z) \left[1 - \sum_k g_{km}(E)\,(JS + V\tau_z)\right]^{-1}. \tag{S13}$$

Since

$$\sum_k g_{km}(E) \simeq \int d\xi\, \nu_0 \frac{E + (-)^m\Delta\tau_x}{E^2 - \xi^2 - \Delta^2} = \frac{-\pi\nu_0(E + (-)^m\Delta\tau_x)}{\sqrt{\Delta^2 - E^2}}, \tag{S14}$$

with ν_0 a one-channel density of states at the Fermi level ($\propto 1/(\pi v_F)$) for the conduction electrons, we find that

$$T(E) = \frac{1}{\pi\nu_0} \frac{(\alpha^2 - \beta^2)E + (\alpha + \beta\tau_z)\sqrt{\Delta^2 - E^2} + (-)^m(\alpha^2 - \beta^2)\Delta\tau_x}{(1 - \alpha^2 + \beta^2)\sqrt{\Delta^2 - E^2} + 2\alpha E}, \tag{S15}$$

whose poles give the Shiba state energies[1]

$$E_m = -\Delta \frac{1 - \alpha^2 + \beta^2}{\sqrt{(1 - \alpha^2 + \beta)^2 + 4\alpha^2}}, \tag{S16}$$

where $\alpha = JS\pi\nu_0 > 0$, $\beta = V\pi\nu_0$. This expression is the same as the one for the Shiba states induced by an exchange potential of the form of a δ-function. The difference is that the Shiba states obtained here are fivefold degenerate.

---

[1] J as defined here differs from the J in the real-space representation (for s-wave scatterers) $J\psi^\dagger(0)\boldsymbol{\sigma}\psi(0)\cdot\mathbf{S}$ by a normalization factor; however, the value of the dimensionless quantity α remains unaffected.

Table I. Character table for the irreducible representations for group C_{4v} and reducible representation D^+

	E	$2C_4$	C_2	$2\sigma_v$	$2\sigma_d$	linear, rotations		quadratic
A_1	1	1	1	1	1	z		$x^2+y^2,\ z^2$
A_2	1	1	1	−1	−1	R_z		
B_1	1	−1	1	1	−1			x^2-y^2
B_2	1	−1	1	−1	1			xy
E	2	0	−2	0	0	(x,y)	(R_x,R_y)	(xz,yz)
D^+	5	−1	1	1	1			

Table II. Character table for the irreducible representations for group C_{3v} and reducible representation D^+

	E	$2C_3$	$3\sigma_v$	linear, rotations		quadratic	
A_1	1	1	1	z		$x^2+y^2,\ z^2$	
A_2	1	1	−1	R_z			
E	2	−1	0	(x,y)	(R_x,R_y)	(x^2-y^2,xy)	(xz,yz)
D^+	5	-1	1				

Crystal field splitting

Above, the Shiba states were obtained from scattering electrons of an isotropic superconductor off an impurity potential with a certain angular momentum component with $l=2$. Thus, the Shiba states are 5-fold degenerate, and their wave functions resemble the shape of d atomic orbitals. The degeneracy is (partially) removed by the crystal field describing the local environment of the magnetic impurity. The nature of the splitting is essentially determined by symmetry. We briefly summarize the standard results of group theory which govern these splittings for the surfaces of interest in the main text.

The point group symmetries for the Pb(001) and Pb(111) surfaces are C_{4v} and C_{3v} with the corresponding character tables in Tables I and II, respectively [3]. As long as the adsorption sites respect this symmetry, we can then read off the generic multiplicities of the Shiba states. In our experiments, we find this to be the case for the Pb(001) surface as well as the for $\mathrm{Mn}^{\mathrm{up}}_{\mathrm{Pb(111)}}$ site on the Pb(111) surface. If the adsorption site further reduces the symmetry, the Shiba states will split even further. In our experiments, we conclude that this is the case for the $\mathrm{Mn}^{\mathrm{down}}_{\mathrm{Pb(111)}}$ adsorption site.

For the case that the absorption sites respect the symmetry of the surface, we thus find from the character tables:

- Pb(001):

$$D^+ = A_1 \oplus B_1 \oplus B_2 \oplus E. \tag{S17}$$

  d_{xz} and d_{yz} orbitals are doubly degenerate, and d_{xy} , $d_{x^2-y^2}$ and d_{z^2} are nondegenerate.

- Pb(111):

$$D^+ = A_1 \oplus 2E. \tag{S18}$$

  $d_{x^2-y^2}$ and d_{xy} are degenerate. d_{xz} and d_{yz} are degenerate. d_{z^2} is non degenerate.

EXPERIMENTAL DATA

$\mathrm{d}I/\mathrm{d}V$ maps with full contrast and at negative bias voltages

In Fig. 3 of the main text we provided $\mathrm{d}I/\mathrm{d}V$ maps at positive bias voltages for a Mn adatom in the $\mathrm{Mn}^{\mathrm{down}}_{\mathrm{Pb(111)}}$ and in the $\mathrm{Mn}^{\mathrm{up}}_{\mathrm{Pb(111)}}$ adsorption site. The contrast of some of the maps was stretched to emphasize the long-range patterns of the YSR states. For completeness, we provide the same maps with a linear color scale in Fig. S1 ($+\alpha$ to $+\epsilon$ and $+\zeta$ to $+\theta$). We provide also $\mathrm{d}I/\mathrm{d}V$ maps of the YSR resonances at negative bias voltages, which show patterns similar to those at positive voltages.

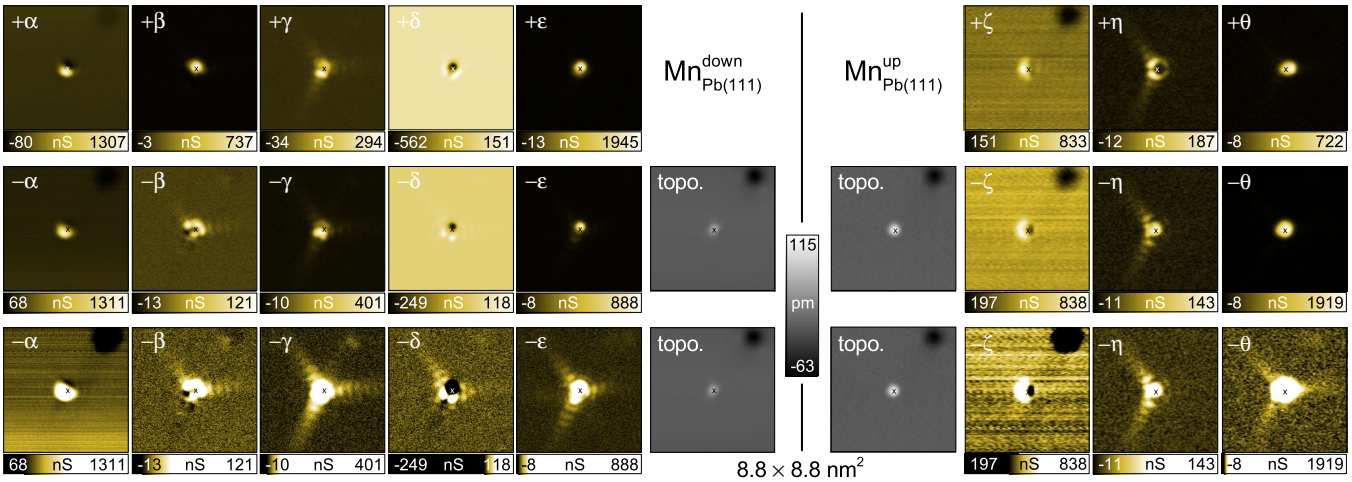

Figure S1. dI/dV maps of a Mn adatom on Pb(111) in the two adsorption sites denoted by $\mathrm{Mn}^{\mathrm{down}}_{\mathrm{Pb(111)}}$ ($\pm\alpha$, $\pm\beta$, $\pm\gamma$, $\pm\delta$, $\pm\epsilon$) and $\mathrm{Mn}^{\mathrm{up}}_{\mathrm{Pb(111)}}$ ($\pm\zeta$, $\pm\eta$ $\pm\theta$), respectively. The corresponding topographies are shown. $\times$ denotes the same position in all maps. The dI/dV maps are recorded with the tip-sample distance adjusted in each pixel to a setpoint of 400 pA at 5 mV. Lock-in modulation: 20 $\mu\mathrm{V}_{\mathrm{rms}}$. The maps of $+\alpha$ to $+\epsilon$ and $+\zeta$ to $+\theta$ reproduce the same data as in Fig. 3 (e,f) of the main text, but with a linear color scale. The maps of the negative energy resonances $-\alpha$ to $-\epsilon$ and $-\zeta$ to $-\theta$ are shown with a linear (top) and with a stretched (bottom) color scale, respectively. Note that the dark spot in the top right corner of the imaged area is a subsurface neon inclusion [4].

Further arguments for the orbital assignment

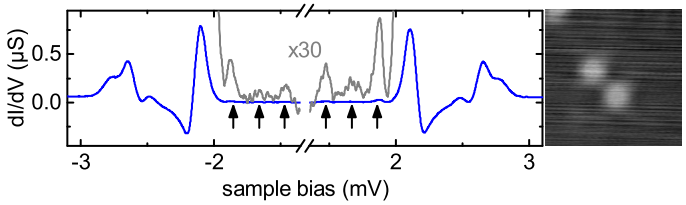

Figure S2. dI/dV spectrum recorded at a pair of adatoms, which lie at close distance. Splitting of the states reveals three resonances close to the original energy of $\pm\gamma$ (marked by arrows). Setpoint: 4 mV at 200 pA. Lock-in modulation: 15 $\mu\mathrm{V}_{\mathrm{rms}}$.

In the main text we deduced the symmetry of the scattering potential from the spatial pattern of the YSR-states observed in the dI/dV maps of a Mn adatom on Pb(001). We assigned the distinct states α, β and γ to originate from scattering of the Mn adatom's d-orbitals. The assignment of resonances $\pm\beta$ to d_{z^2} was unambiguous because the intensity is strongest at the center of the adatom and only weak into the $\langle 110\rangle$ directions. Resonances α and γ originate either from scattering at $d_{\mathrm{x}^2-\mathrm{y}^2}$ and/or from the orbitals $d_{\mathrm{xz,yz}}$ and d_{xy}. An assignment from the spatial shape of the YSR state alone is ambiguous. At higher coverage, we also observe pairs of adatoms at close distance. The interaction leads to a splitting of the resonances $\pm\gamma$ into three pairs of resonances [see Fig. S2]. This requires $\pm\gamma$ to actually consist of (at least) two resonances. Thus, we assigned $\pm\gamma$ resonances to scattering at the orbitals $d_{\mathrm{xz,yz}}$ and d_{xy}, which are degenerate in the single atom. Resonances $\pm\alpha$ then originate from scattering at $d_{\mathrm{x}^2-\mathrm{y}^2}$.

Lateral decay of dI/dV intensity

In the main text we showed the lateral decay of spectral intensity of YSR states along the $\langle 110\rangle$ high-symmetry directions in the vicinity of a $\mathrm{Mn}^{\mathrm{up}}_{\mathrm{Pb(111)}}$ adatom. The curves were extracted from high-resolution dI/dV maps at the energies of the YSR states. To emphasize the oscillatory intensity variations, we subtracted a background $b(r)$, which is derived from the $1/r$ dependence of the YSR wavefunction $\psi(r)$ at distances $r < \xi$ (ξ is the coherence length of the superconductor):

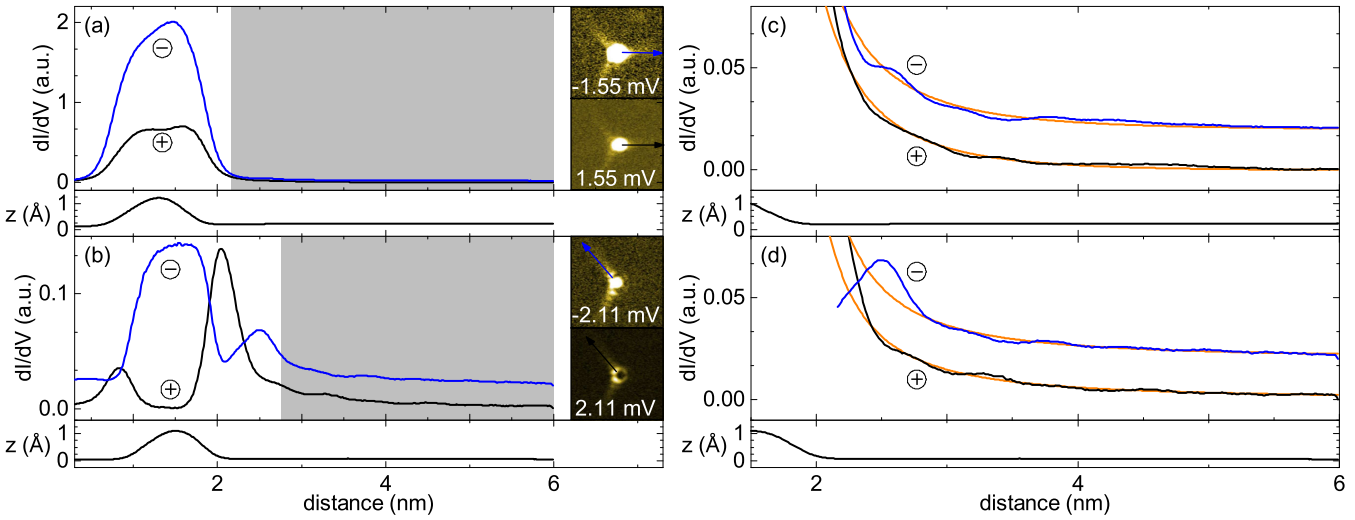

Figure S3. Lateral decay of the spectral intensity at positive (black) and negative bias (blue) of the two YSR resonances with lowest binding energy for an adatom on Pb(111) in the $\mathrm{Mn}^{\mathrm{up}}_{\mathrm{Pb(111)}}$ adsorption site. Setpoint: 400 pA, 4 mV. Lock-in modulation: 20 μV. The blue curves in (c,d) are offset for clarity by 0.02. (a,b) show the full profiles as extracted from high-resolution dI/dV maps along the ⟨110⟩ crystal directions. (c,d) show a zoom of the gray shaded areas in (a,b). Removal of the strongly decaying background, which is shown as orange line, leads to Fig. 3 of the main text. The z profiles show the apparent height as a function of distance from the impurity center.

$$b(r) = \left| y_0 + \frac{1}{k\,|r - r_0|} \right|^2 . \tag{S19}$$

Here, k and y_0 are independent fit parameters, and r_0 is set to the center of the adatom. Figure S3 shows the full datasets of the spectral intensity at positive and negative bias in (a,b). The region of interest is shaded with a gray background, and displayed in (c,d). Subtracting the decay function (orange) leads to Fig. 3 of the main text.

[1] J.R. Schrieffer, J. Appl. Phys. **38**, 1143 (1967).
[2] A.M. Tsvelick, P.B. Wiegmann, Adv. Phys. **32**, 453 (1983).
[3] M.S. Dresselhaus, G. Dresselhaus, A. Jorio, *Group Theory: Application to the Physics of Condensed Matter*, (Springer, 2007).
[4] M. Ruby, B.W. Heinrich, J.I. Pascual, and K.J. Franke, Phys. Rev. Lett. **114**, 157001 (2015).